On the Importance of Nuclear Quantum Motions in Near Edge X-ray Absorption Fine Structure (NEXAFS) Spectroscopy of Molecules

Craig P. Schwartz[1,2], Janel S. Uejio[1,2], Richard J. Saykally[1,2], David Prendergast[3]*

1. Department of Chemistry, University of California, Berkeley

2. Chemical Sciences Division, Lawrence Berkeley National Laboratory

3. Molecular Foundry, Lawrence Berkeley National Laboratory

* Corresponding Author - E-mail: dgprendergast@lbl.gov

Phone : (510) 486-4948

Fax : (510) 486-7424

Abstract

We report the effects of sampling nuclear quantum motion with path integral molecular dynamics (PIMD) on calculations of the nitrogen K-edge spectra of two isolated organic molecules. *S*-triazine, a prototypical aromatic molecule occupying primarily its vibrational ground state at room temperature, exhibits substantially improved spectral agreement when nuclear quantum effects are included via PIMD, as compared to the spectra obtained from either a single fixed-nuclei based calculation or from a series of configurations extracted from a classical molecular dynamics trajectory. Nuclear quantum dynamics can accurately explain the intrinsic broadening of certain features. Glycine, the simplest amino acid, is problematic due to large spectral variations associated with multiple energetically accessible conformations at the experimental temperature. This work highlights the sensitivity of NEXAFS to quantum nuclear motions in molecules, and the necessity of accurately sampling such quantum motion when simulating their NEXAFS spectra.

Keywords - PIMD, NEXAFS, Gas phase, Herzberg-Teller, Nitrogen K-edge, XANES

1. Introduction

Core level spectroscopies are unique and powerful atom-specific probes of molecular interactions via both occupied and unoccupied electronic states.[1] As methods involving x-ray absorption (XAS, NEXAFS, XANES) or x-ray photo-electron spectroscopy (XPS) mature, they are increasingly being applied to complex molecular systems, including proteins, DNA, large organic molecules and polymers.[2] However, a major limitation is that deriving molecular information from these measurements usually depends explicitly on comparison with theoretical calculations, which are extremely difficult to perform at the accuracy of modern experiments. The accurate description of an absorption event of several hundred electron-volts of energy is an ongoing challenge in theoretical chemistry. Our work indicates that these calculations are extremely sensitive to the molecular geometries; therefore, in addition to an accurate theoretical formalism to describe the spectroscopy, the molecular geometries and their thermal fluctuations must be correctly sampled.[3] Herein, we describe the importance of quantum vibrational effects on core level excitations of the nitrogen K-edge of gas phase *s*-triazine and glycine. This is relevant to both near edge x-ray absorption fine structure (NEXAFS) and inner shell electron energy loss spectroscopy (ISEELS).

It has been shown previously that density functional theory (DFT) [4] can accurately reproduce excitation energies associated with core-level spectra via total energy differences (ΔSCF or ΔKS).[5] We use this to our advantage to model the core hole caused by the absorption of an x-ray photon; we represent the lowest energy core-level excited state self-consistently using a full electronic core hole on the excited atom and an associated screened excited electron (XCH).[6]

XCH differs from the closely related full core hole (FCH) approximation, which ignores the excited electron entirely or replaces it with a uniform background charge density (in the case of periodic systems),[7] and from the half core hole (HCH) approach, in which one removes half an electron from the system.[8,9] Another approach is an efficient cluster-based multiple scattering method, often used for heavier elements; this method is difficult to extend to lighter atoms, particularly those with a smaller atomic number than aluminum.[10] Shirley has developed accurate methods for solving the Bethe-Salpeter equation for crystalline solids, however, this high level of accuracy comes at significant computational cost.[11] Others have applied multi-electron quantum chemistry to simple systems, but generally these methods scale poorly with system size.[12] Another approach is static exchange, which freezes the orbitals of the molecular ion and calculates their exchange energy with the excited electron within a quantum calculation;[13] however this does not include the self-consistent relaxation of valence electrons due to the presence of the excited electron, which can have a significant impact on the relative energy and character of certain transitions. Recently, Ågren and coworkers have developed a polarization propagator approach, which has the significant advantage of not having to address specific atom-centered excited states explicitly.[14] While this method is extremely promising, an implementation using plane waves or a real space numerical grid is not yet available and may be difficult due to a variety of issues related to accurately representing both localized core and extended valence states within the same computational framework.

Methods based on linear combinations of atomic orbitals (LCAOs) are highly successful in representing localized bound states.[5] However, LCAOs are limited in their ability to accurately describe delocalized scattering events, which become particularly important for electronic excitations to states above the ionization potential.[15] Thus, we have chosen to use

plane waves, which are capable of approximating equally well both localized and scattering states.[3] We approximate the high energy continuous electronic density of states by exploiting the periodic boundary conditions of our supercell calculations and numerically converging an integration in k-space over the first Brillouin zone (BZ).[3]

All of these methods require a structural model for the molecules. In general, the most common approach is to calculate the lowest energy structure by holding the electrons in their quantum ground state while modeling the atomic nuclei as classical point charges, herein referred to as the fixed-nuclei approximation.[3,16] This is clearly a poor approximation if the molecule is not populated exclusively in its nuclear ground state, and for that reason, others have investigated the importance of multiple low-energy conformers.[17] Ågren and coworkers employ a more thorough approach, deriving excited-state potential energy surface gradients and using these for calculations of Franck-Condon factors.[18] This approach becomes prohibitively expensive for large molecules and impracticable for those with multiple low energy conformations or highly anharmonic motion. Furthermore, this approach neglects the impact of nuclear motion on the electronic transition amplitude; to first order, this impact is referred to as the Herzberg-Teller effect.[19] Attempts have been made to treat atomic movements directly in XAS by approximating thermal motions with Debye-Waller factors.[20] This assumes that all the molecules will move in harmonic potentials of width matched to experimental conditions; this will likely have limited validity for isolated molecules, particularly if they exhibit large conformational changes.

We have previously investigated improvements in simulating XAS using a classical trajectory, rather than using the usual fixed-nuclei approximation.[3] Large spectral changes were observed based on these classical thermal motions. Herein, we investigate the changes produced

in simulated NEXAFS of molecules at the nitrogen K-edge when treating nuclear motions quantum mechanically by using path integral molecular dynamics (PIMD). These molecules are s-triazine, a relatively rigid prototypical ring structure, and glycine, the simplest amino acid. PIMD, based on the Feynman path integral formalism,[21] treats the atomic nuclei as quantum, rather than classical particles. We find that sampling quantum nuclear motions can induce large spectral changes in NEXAFS spectra, more accurately predicting certain features at a cost of some additional configurational sampling.

This is not the first work to note the importance of quantum fluctuations on electronic structure and associated spectroscopy. Earlier work simulated the gas phase valence electronic spectra of lithium clusters[22] and hydrazine.[23] In the hydrazine study, due to the efficiency of the algorithm employed and the use of localized basis set, extensive sampling was possible using an ab initio potential surface coupled with time dependent DFT.[23] Our work differs in that it explores the x-ray region of the spectrum where, as we shall see, localized basis sets are insufficient to describe high energy scattering states.

2. Computational Methods

X-ray absorption

We calculate the x-ray absorption cross section to first order using Fermi's golden rule:

$$\sigma(\omega) = 4\pi^2 \alpha_0 \hbar\omega \sum_f |M_{i \longrightarrow f}|^2 \delta(E_f - E_i - \hbar\omega) \qquad \textbf{Equation 1}$$

Here $\hbar\omega$ is the energy of the incident photon, which should match the difference in energy between the final and initial states $E_f - E_i$; α_0 is the fine structure constant. $M_{i \to f}$ are the transition amplitudes between initial and final states, evaluated within the dipole approximation using a single-particle approximation

$$M_{i \longrightarrow f} = < \Psi_f | \hat{\varepsilon} \bullet R | \Psi_i > \approx S < \psi_f | \hat{\varepsilon} \bullet r | \psi_i >, \qquad \textbf{Equation 2}$$

where $\hat{\varepsilon}$ is the polarization direction of the photon electric field and $|\Psi_{i,f}\rangle$, **R** are the many-electron initial and final states and position operator, respectively, and their lower-case versions correspond to single-electron analogues. We approximate the prefactor $S \leq 1$ as constant over all single-particle transitions.[6] In this work, the single-particle eigenstates and eigenvalues are non-interacting Kohn-Sham states as computed by density functional theory within the generalized gradient approximation. We use the PBE form of the generalized gradient approximation to the exchange-correlation potential.[24]

For x-ray core hole excitations at the nitrogen K-edge, the intial state $|\psi_i\rangle$ is fixed to the 1s atomic eigenstate of nitrogen (calculated for the ground state electronic configuration using PBE). For reasons which will become clear below, we adopt a plane-wave representation and pseudopotential approximation for valence electronic structure. The excited state was approximated to be spin-unpolarized. In all of our calculations, we use norm-conserving pseudopotentials with a numerically converged plane-wave cut-off of 85 Rydberg. These valence pseudostates are smooth, nodeless functions of position in the neighborhood of atomic nuclei, and consequently do not possess the correct overlap with particular atomic core states relevant to x-ray excitations. To fix this, we adopt a frozen-core approximation and augment the core-region

of each valence state using projections of well-defined angular momentum about the atomic site of interest,[25,26] as follows:

$$\left\langle \psi_f \left| \hat{\boldsymbol{\varepsilon}} \bullet \mathbf{r} \right| \psi_i \right\rangle \approx \left\langle \tilde{\psi}_f \left| \sum_{\lambda} \left| \beta_{\lambda}^{N_I} \right\rangle \left\langle \phi_{\lambda}^{N_I} \right| \hat{\boldsymbol{\varepsilon}} \bullet \mathbf{r} \right| \phi_{1s}^{N_I} \right\rangle \qquad \textbf{Equation 3}$$

In this expression, $\left| \tilde{\psi}_f \right\rangle$ is the pseudo (nodeless) final state and $\left| \phi_{1s}^{N_I} \right\rangle$ is the 1s atomic core state at the site of nitrogen atom I. We project the relevant core-region of $\left| \tilde{\psi}_f \right\rangle$ employing a sum of atomic projections $\left| \beta_{\lambda}^{N_I} \right\rangle$ with composite angular momentum index $\lambda = (l, m)$ and augment this core-region using associated all-electron (with nodes) atomic valence states $\left| \phi_{\lambda}^{N_I} \right\rangle$. In the case of 1s core excitations, this sum over projections is limited to dipole-allowed p-projections. This expression is computationally inexpensive to evaluate: the all-electron atomic dipole matrix elements are calculated on the same log-radial grid used in the pseudopotential generation and can be stored and reused for all nitrogen K-edge calculations within the given approximation to the DFT exchange-correlation potential; the angular momentum projections are just those used to calculate the non-local potential matrix elements of the Kohn-Sham DFT Hamiltonian within the plane wave implementation. Note that for first-row elements, the pseudopotential p-channel is often chosen as local, and therefore has no associated projector within the norm-conserving Kleinman-Bylander formalism. In this case, the use of an ad hoc localized projector is necessary.[25]

XCH Approach

To approximate the electronic final state within our Fermi's Golden Rule expression (1) we adopt the eXcited state Core Hole (XCH) approximation. The core-level excited state of the molecule is approximated by replacing the pseudopotential of the core-excited atom with one which explicitly includes a core-excitation – for nitrogen we use the electronic configuration:

$1s^1 2s^2 2p^4$. We also include the important screening presence of the excited electron, by incrementing the number of ground state valence electrons by one. We then generate a self-consistent set of Kohn-Sham valence states in the presence of both of these perturbations. The atomic nuclei remain fixed in place as they will not move appreciably on the attosecond time scale of this excitation. The resulting constrained DFT ground state of this perturbed system is well-defined and approximates the first core-excited state. We further approximate higher excited states by using the unoccupied Kohn-Sham spectrum of this XCH self-consistent field. (We acknowledge that this approach may incorrectly describe the screening of excited states of different character than the first excited state, however, we welcome the convenience of an orthonormal set of final states provided by our approach.)

Challenges for molecular systems – localized vs. continuum states, supercells.

The use of plane-wave basis sets to model the electronic structure of isolated molecules requires the use of large supercells within periodic boundary conditions. Large cells are used ($(20\ \text{Å})^3$) to reduce spurious interactions between cells and so as to be large enough to represent excited states below the ionization potential (IP). In all cases except PIMD, approximately 100 Kohn-Sham eigenstates are used in constructing transition matrix elements, sufficient to extend the spectra approximately 3 eV above the estimated IP; for the PIMD calculations 250 Kohn-Sham eigenstates are used extending the spectra approximately 5 eV above the IP. Due to the large box size, and hence reduced energy spacing between electronic bands, a large number of unoccupied states are needed to describe high-energy transitions. The zone-center electronic structure is calculated using the PWSCF code.[27]

We take full advantage of the periodic boundary conditions to approximate the continuum of electronic states found at high energy by numerically converging an integration over the

Brillouin Zone (BZ). This should not affect states that are contained entirely within a given supercell. For states which are larger than a given supercell, the electronic density of states can be reasonably determined by BZ sampling.[28] These delocalized states are similar to the unbound electronic states scattered from the molecule. The weakness of such a technique is in describing localized bound states lying below the ionization potential with spatial extents larger than the chosen supercell; we minimize this effect by using very large supercells.

In order to mitigate the computational cost of numerically converging the BZ integral, we utilize a technique developed by Shirley.[29] In our implementation of this technique for molecules, we require only the electronic structure at the zone center (k=0) as input, yet we can generate eigenvalues and eigenstates to meV accuracy throughout the BZ within the energy range of the states provided at the zone center. This interpolation technique exploits the slow variation in the Bloch periodic part of the eigenfunctions $\left|u_{nk}\right\rangle = e^{-ik.r}\left|nk\right\rangle$ with respect to k. An optimal basis is constructed from a coarse sampling of these $\left|u_{nk}\right\rangle$ across the BZ, diagonalizing the overlap matrix of these functions and discarding those eigenvectors having very small eigenvalues, thereby removing linear dependence. The k-dependent Hamiltonian is expressed in this basis. For eigenstates with energies beyond those of the input coarse sampling of the BZ, we cannot guarantee the accuracy of this interpolated Hamiltonian. However, we notice some transferability to higher energies, and the resulting spectra at very high energies appear to improve with averaging over the thermodynamic ensemble (see results).

Nuclear geometry considerations

Generally, core-level spectra of isolated molecules are simulated within the fixed-nuclei approximation,[5] particularly for molecules in their vibrational ground state under experimental conditions. The lowest energy structure is computed treating the electronic structure quantum

mechanically but modeling the atomic nuclei as fixed point charges. We performed this minimization on both the molecules studied here. For molecules not in their ground state, a Boltzmann weighted average of significant conformers is often used to attempt to generate the experimental spectrum.[17] We have calculated this for glycine. Unfortunately, as we will show this proves to be inadequate to properly describe the measured broadening. Structures which are not at significant conformational minima can have large spectral contributions.

In order to explicitly account for the motions caused by temperature, we have modeled the nuclear degrees of freedom in these molecules using molecular dynamics (MD) performed at 300 K with a Langevin thermostat utilizing the generalized AMBER force field and Antechamber. [30] The resulting distribution of nuclear coordinates is spaced at least 10 picoseconds apart to eliminate correlation between configurations for at least 100 configurations. The correlation was estimated at under 5 picoseconds for both molecules. Empirical, rather than *ab initio*, force fields were used in order to avoid the computational bottleneck associated with generating uncorrelated sampling. Due to NEXAFS relative insensitivity to bond lengths it is believed that this approximation of using empirical rather than *ab* initio should be relatively minor compared to various other approximations. Our tests indicate that the structural parameters derived from the AMBER potential agree with DFT results within ~2%.

Quantum vs. Classical Distributions

One problem with using classical MD is that this is based on Newton's classical equations of motion for the atomic nuclei, and should fail for quantum systems, in particular for a molecule like *s*-triazine which is largely in its vibrational ground state at the experimental temperature. This is evident from the vibrational spectrum of s-triazine shown in Table I, which was calculated using Gaussian 03.[31] Therefore, in addition to our classical MD simulations, we

have performed path integral molecular dynamics (PIMD)[21] for both glycine and *s*-triazine, in order to generate a quantum distribution of states. Path integral molecular dynamics has been used extensively by groups in the past to simulate gases, liquids and solids.[22,23,32,33] Often large differences are found based upon using quantum descriptions of molecules versus those that treat molecules classically.[23,32] We note previous work has been done using PIMD to explain certain populations of glycine conformations.[34] This is not the first work to note the importance of quantum fluctuations on spectra for electronic transitions. Previous work has explored the importance of quantum motion to valence excitations.[22,23] In general, core hole excitations should be more sensitive to changes in structure or symmetry for small molecules.

Our PIMD simulations use the same classical potentials and the same Langevin thermostat used in the classical simulations, PIMD samples the nuclear quantum distribution using a chain of coupled "quantum beads;" we used 32 beads per atom at 300K, the same temperature as was used classically. Following a 1 nanosecond equilibration, the simulations were run for 10 nanoseconds. As will be seen in the results, significant spectral deviations are seen between the calculated PIMD spectra and the calculated classical MD spectra. These significant spectral deviations were also seen for glycine, which should not be in its nuclear ground state at the experimental temperature. The calculated vibrational frequencies of glycine are provided in Table II. The lowest vibrational frequency corresponds to less than 100K.

For *s*-triazine, four uncorrelated configurations were selected from a PIMD trajectory, and the electronic structure of all 32 bead sets were used as the starting geometries for electronic structure calculations. This sampled a total of 128 nuclear geometries. In the case of glycine, a single bead set was followed through 100 well-spaced configurations and used as the nuclear coordinates for DFT calculations. Only one bead was used for glycine in an attempt to sample

more of the conformational space; sampling all 32 bead sets (requiring 3200 spectra) would have been prohibitively expensive to compute. Selecting 4 configurations and calculating all 32 bead sets in a manner similar to s-triazine would have provided much less sampling of conformational space. The computational bottleneck of our approach is in the XCH calculations since generating 100 uncorrelated configurations from PIMD at intervals well beyond the auto-correlation time requires only on the order of 1% of the time of the 100 XCH calculations. We note that the structural ensembles were converged by running the simulations for an extended period of time, but only ~100 configurations of those trajectories were sampled by XCH. These XCH calculations were performed on the Franklin supercomputer at NERSC.

Spectral alignment across configurations

These DFT/XCH calculations produce a set of Kohn-Sham eigenvalues and associated transition probabilities which may be numerically broadened to produce a smooth spectrum for a range of energies. However, the energy scale of the eigenvalues in these pseudopotential XCH calculations will be offset from the true energy scale of such core-level excitations in experiment and this must be adjusted in a systematic way. For the K edges of light elements, the energy of the measured absorption onset $E_{onset}^{\exp}$ is typically quite sharp and so, one might align the energy of the occupied LUMO state of the XCH with the experimental onset. This would correspond to shifting the energy scale as follows:

$$E \mapsto E - \varepsilon_{LUMO}^{XCH} + E_{onset}^{\exp}.$$

Equation 4

Such an alignment has been common practice for pseudopotential calculations. In this work we take a slightly different approach, choosing to align to the measured ionization potential ($IP_{\exp}$) instead. The purpose of such an alignment is to provide an unambiguous separation

between bound and continuum states and to remove possible ambiguities arising from DFT's underestimation of bandwidths. Estimating the IP is also complicated when using pseudopotentials, and so, instead, we estimate the relative position of the absorption onset below the IP using the difference $E_{tot}^{FCH} - E_{tot}^{XCH}$. The full core hole approximation is used to model the core-ionized molecule. Now the resulting shift in the energy scale is

$$E \mapsto E - \varepsilon_{LUMO}^{XCH} + IP_{\exp} - (E_{tot}^{FCH} - E_{tot}^{XCH}).$$

Equation 5

All of this applies to an individual molecular configuration. However, if we wish to align the spectra of different molecular configurations (for the purpose of ensemble averaging) then we adopt the following procedure. One molecular configuration is chosen as a reference, denoted by 0 (in this work we chose the fixed-nuclei structure), and the shift of its eigenvalues derives from Eq. 5 above:

$$E(0) \mapsto E - \varepsilon_{LUMO}^{XCH}(0) + IP_{\exp} - [E_{tot}^{FCH}(0) - E_{tot}^{XCH}(0)] = E - \varepsilon_{LUMO}^{XCH}(0) + \Delta(0) .$$

Equation 6

This assumes that the ionization energy of the fixed-nuclei structure sits at the same position as the peak in the experimental x-ray photoemission spectrum (nominally referred to as the IP). In general, the error associated with such an alignment (typically ~0.1eV) is less than the inherent underestimation of band widths in our DFT calculations. For particularly asymmetric XPS peaks, the alignment may require some adjustment.

For another molecular configuration (i), we must include a further shift relative to the reference (0), derived as follows: The core-excitation energy (in an all-electron formalism) is approximated as $E_{tot}^{XCH} - E_{tot}^{GS}$, the total energy difference between core-excited and ground states. The relative energy of excitations on different molecular configurations is

$$\begin{aligned} \Delta_r(i) &= [E_{tot}^{XCH}(i) - E_{tot}^{GS}(i)] - [E_{tot}^{XCH}(0) - E_{tot}^{GS}(0)] \\ &= [E_{tot}^{XCH}(i) - E_{tot}^{XCH}(0)] - [E_{tot}^{GS}(i) - E_{tot}^{GS}(0)] \end{aligned} .$$

Equation 7

Note that this rearrangement also enables us to compute meaningful energy differences within pseudopotential calculations and so, the ultimate shift applied to eigenvalues of configuration (i) is

$$E(i) \mapsto E - \varepsilon_{LUMO}^{XCH}(i) + \Delta_r(i) + \Delta(0) .$$

Equation 8

Clearly, an analogous expression to Eq. 7 exists for providing the relative alignment of spectra coming from inequivalent atoms of the same species in a given molecular configuration. In this special case, the ground state energy differences are zero.

We wish to emphasize the importance of such shifts when combining spectra from a large set of molecular configurations to provide an ensemble average -- they are vital. Without them we obtain meaningless results. In particular, $\Delta_r(i)$ provides an accurate estimate of how well the environment/configuration can screen the core-excitation. This approach to energy alignment across molecular configurations has also been adopted in our previous work.[3,6] We note that the use of total energy differences in constructing relative alignment is compatible with the original ΔSCF motivation behind using the XCH approximation, which runs contrary to other approaches based on eigenvalue differences.

Spectral impact of vibrations

Variations in the nuclear degrees of freedom of molecules unsurprisingly have noticeable impacts on electronic structure in terms of shifting energy levels and modifying the symmetry of electronic states. In terms of the associated spectra, features may move in energy and change in intensity. We can analyze such effects within the Born-Oppenheimer approximation, assuming that electronic and nuclear states are decoupled:

$$|\Psi>=|\psi>\times|\chi> \qquad \textbf{Equation 9}$$

where $|\psi>$ is an electronic state and $|\chi>$ is a vibrational state. We explore the impact of small nuclear displacements along normal modes Q_ν on the transition amplitudes, $M_{i\to f}$ from initial state i to final state f, where

$$M_{i\longrightarrow f} = \mu_{n_i\longrightarrow n_f} < \chi_{\nu_i} | \chi_{\nu_f} > + \sum_{\nu=1}^{3N-6} \frac{\partial \mu_{n_i\longrightarrow n_f}}{\partial Q_\nu} < \chi_{\nu_i} | Q_\nu | \chi_{\nu_f} > + O(Q^2)$$

Equation 10

Here, $\mu_{n_i \longrightarrow n_f} = < \psi_{n_i} \mid r \mid \psi_{n_f} >$, corresponds to a dipole transition between an initial and final electronic electronic state; $< \chi_{v_i} \mid \chi_{v_f} >$ corresponds to the overlap of the initial and final vibrational modes. The modulation of the first term in this expansion, due to overlap of vibrational states on the ground and excited state potential energy surfaces, is the well-known Franck-Condon effect. The term linearly dependent on the normal coordinates Q_v corresponds to the Herzberg-Teller effect.[19] The Franck-Condon approximation states that because the nuclei are so much more massive than electrons, an electronic transition takes place before the nuclei can respond. Therefore, the transition probability will rise with increasing spatial overlap between the initial and final state wavefunctions. The Herzberg-Teller effect expresses that the transition intensity can change with the coordinates. For a molecule that moves far from its minimum energy positions, such as glycine at room temperature, we find this effect to be spectrally significant. Clearly, for dipole forbidden transitions, the Franck-Condon term is negligible and, in the presence of symmetry-breaking nuclear displacements, the Herzber-Teller term will dominate.

The central assumption behind the Born-Oppenheimer approximation implies that the time-scale of electronic transitions is much faster than nuclear motion, and for core-level excitations, we make the assumption that the probe can instantaneously sample the nuclear coordinates. In effect, the x-ray or electron beam takes configurations of a large ensemble of molecules, each with their nuclear degrees of freedom displaced to some degree from their mean positions.

We note that there are existing approaches which explore the vibrational degrees of freedom within a normal mode analysis, generating accurate Franck-Condon factors. However, such analysis neglects the Herzberg-Teller effect and higher order terms in Eq.10.

Our technique of generating a quantum distribution of conformations by MD sampling, and then using these displaced structures as the nuclear coordinates for electronic structure calculations, has advantages over other techniques. In particular with our approach, in the limit of infinite sampling, we expect to describe the Herzberg-Teller effect in addition to all the higher order effects.

All calculated transitions are numerically broadened using Gaussians of 0.2 eV full width at half maximum. We use this relatively small and uniform broadening with the aim of simulating and distinguishing electronic and vibrational effects explicitly. Certain features of spectra result from the fundamental energy dispersion of certain electronic states or the short lifetime of certain transitions, while other features will be caused by the motions of the molecules.[1,3] We believe that purposely using a small numerical broadening permits a predictive computational approach which can distinguish between electronic broadening and vibrational broadening of spectral features.

3. Results and Discussion

S-triazine

S-triazine ($C_3N_3H_3$) is a small, naturally occurring prototypical aromatic molecule; it consists of a resonant ring, analogous to benzene, with alternate carbon atoms replaced with nitrogen atoms, giving it a high level of symmetry (D_{3h}). At room temperature, the molecule is localized largely in its ground vibrational state, see Table I. Figure 1 (a) shows the molecular structure of *s*-triazine along with its calculated spectra at the nitrogen K-edge using various

approaches to sampling the nuclear degrees of freedom, with Figure 1 (b) focusing on the energy range from 398 eV to 403 eV. The inner-shell electron energy loss spectroscopy (ISEELS) and NEXAFS spectra are taken from the literature, as is the measured experimental ionization potential.[12,16,35] The theoretical results are aligned to the experimental ionization potential, as described in section 2. The fixed nuclei and classical MD results have been shown previously.[3] The measured spectra comprise six features which have been previously assigned as follows: (1) a HOMO to LUMO π^* transition; (2) a shoulder to the first feature, also due to a π^* transition, which is turned on by vibronic symmetry-breaking; (3) a feature which has previously been assigned to mixed Rydberg states; (4) a multiple electron peak, definitively assigned recently by Duflot *et al.*; (5) and (6) peaks believed to be σ^* in character.[12,16,35] The energy positions of these 6 features are listed in Table III. We now provide an assessment of the accuracy of the various theoretical approaches employed in this work.

The fixed nuclei spectrum approximation overestimates the intensity of feature 1, with features 2 and 4 missing, but obtains features 3 and possibly 5. Using classical MD lead to a decrease in the intensity of feature 1, in better agreement with experiment, while agreement for peaks 3 and 5 are improved. The shoulder (feature 2) is visible as an error bar, while features 4 and 6 are missing entirely. Classical molecular dynamics samples changes in atomic structure and the subsequent changes in electronic structure which, to first order, are described by the Herzberg-Teller effect. This is crucial in generating the second feature, which results from symmetry-breaking vibrational modes, as described in Ref. 4. Classical molecular dynamics does not adequately reproduce the intensity of feature 2. Furthermore, our calculations simulate single-electron transitions only, and so we would not expect to calculate feature 4 at all, which has been assigned definitively by Duflot *et al.* as a multielectron feature.[12,16,35]

PIMD shows a substantial improvement in the ability to predict the *s*-triazine spectrum. The first peak is accurately reproduced in terms of relative intensity, and significantly, the second feature, previously assigned to vibronic effects, is clearly visible as a shoulder, in contrast to the classical MD sampled spectra where the second feature was seen only as a non-zero sampling error bar. The PIMD spectra gives the onset feature an asymmetry similar to that of experiment, including the long tail evident in the experiment at the edge of feature 2 (Fig. 1 (b)). Features 3 and 5 are in agreement with the previous computed spectra, and notably, feature 6 is also obtained. The improvement in agreement and the appearance of new features is due to the increased vibronic symmetry breaking associated with PIMD. The use of the classical AMBER potential together with PIMD reasonably samples the quantum distribution of states necessary to reproduce the spectrum, with all the single electron features accurately captured.

Both classical MD and PIMD underestimate the energy width of all features due (we expect) to the underestimation of bandwidth typical in DFT approximations.[3] However, PIMD provides a much more general route to accurately obtaining spectra – at least for small molecules. In the particular case of the highly symmetric *s*-triazine molecule, there are clear selection rules for electronic transitions which may be broken by nuclear motion. A probe which can induce such transitions (x-ray) on a time scale faster than the period of nuclear vibrations allows the indirect observation of these displacements via their associated symmetry breaking. In general, for systems with lower symmetry or heavier, less mobile nuclei, this effect may not be so noticeable in core level spectroscopy.

Shown in Figure 2 are the isosurfaces of some DFT Kohn-Sham eigenstates from the electron density of the fixed-nuclei geometry without and with a core hole and from a single configuration taken from the PIMD simulation without and with a core hole placed on the

lowermost nitrogen atom of *s*-triazine respectively. There is a noticeable correspondence between the ground state and the core-excited electronic structure. In Ref. 3, we noted that the presence of nuclear displacements which break symmetry is sufficient to alter the electron density in the vicinity of the core excited nitrogen atom. Electronic transitions to states A and B, the LUMO and LUMO+1 respectively, clearly have π^* symmetry and correspond to features 1 and 2 in the measured spectra. It is worth noting that the LUMO and LUMO+1 are almost degenerate in the electronic ground state; they are separated by less than 10 meV in our DFT calculations. The presence of the core excitation alone is enough to break this degeneracy by 0.7 eV.[3] The further inclusion of vibrations causes electron density to delocalize along the C-N bond, resulting in a reduced intensity of feature 1. Feature 2 appears due to the delocalization of electron density from the neighboring carbon to the core excited nitrogen; this is only enabled by symmetry breaking nuclear motion.[3] Comparing the fixed-nuclei and PIMD electron density when both have a core hole shows that the motion caused by PIMD causes the electron density to shift onto the nitrogen. Several transitions occur in the region of feature 3, one of which is shown in Figure 2C. This particular transition has some σ^* characteristics, but other transitions in the same energy range involve the entire *s*-triazine ring;[3] no simple assignment can be made for this feature as it is due to many different transions.[16,35] One benefit of plane waves is their ability to describe scattering states, such as one of the transitions contributing to feature 5, Figure 2D. Accurately describing such a state using a localized basis set would be problematic.

It has been shown previously that symmetry-breaking can lead to significant spectral changes, in particular, the allowing of previously forbidden transitions.[3] In *s*-triazine, different forms of symmetry breaking can allow different transitions. The large symmetry change caused by the local core excitation lowers the molecular symmetry from D_{3h} to C_{2v}. As described in

Section 2, the additional symmetry-breaking nuclear motion leads to changes in transition amplitudes via the Herzberg-Teller effect.[19] We monitor two such nuclear coordinates here.

We measure changes of in-plane symmetry for *s*-triazine using the difference between the absolute value of two carbon-nitrogen-carbon bond angles (labeled θ_L and θ_R in Figure 3) for one specific nitrogen atom sampled from a long trajectory. Nonzero values correspond to symmetry-breaking. When using classical MD or PIMD, the variance of this measure grows from 5.4° to 14.5°. The higher variance corresponds to more symmetry breaking in the case of PIMD, as compared to the fixed nuclei case, which is symmetric in-plane.

Figure 4 shows another sampled symmetry breaking nuclear coordinate in *s*-triazine – out of plane deformations, measured by tracking the carbon-nitrogen-carbon-hydrogen dihedral deformation; an angle of zero degrees corresponds to a flat molecule. It is clear from the histogram that the amplitude of out of plane deformations increases from classical MD to PIMD. The PIMD sampling of larger nuclear deformations results most noticeably in increased spectral intensity for feature 2 (which is entirely caused by nuclear motion), and generally improves agreement with experiment.

It is important to mention that the error bars shown on all calculated spectra correspond to a standard deviation of the sampled spectra, but this does not correspond to the error in the experiment. The experimental uncertainty derives from a spatial average of the number of instantaneous molecular conformations captured within the x-ray beam, followed by a time average over the duration of the exposure to the beam (both intrinsic uncertainties), followed by repeated measurements to overcome instrument noise. Therefore, all the variance associated with the molecules being in different conformations is encompassed in the huge spatial and temporal sampling per data point obtained experimentally. This sampling is what we attempted

to approximate by using molecular dynamics in this work. What we find is that such sampling is indeed necessary, given the marked differences between spectra computed from the fixed nuclei approximation and using PIMD, and the improved agreement with experiment resulting from using PIMD. In summary, the fluctuations in molecular conformation dominate the calculated spectrum, and by inference, the experimental spectrum.

Glycine

Glycine, (NH_2CH_2COOH), the simplest amino acid, is vibrationally active at the experimental temperature, as can be determined from the vibrational spectrum provided in Table II. Even though the four energetically most stable conformers determined by DFT fix the five heavy atoms in the same plane, glycine has a variety of "soft" modes that enable the nitrogen-containing amine group to rotate relative to the carboxyl group;[17] therefore conformations besides the four most dominant conformers will be populated. The populations of all conformations were monitored by tracking variations in the nitrogen-carbon-carbon-oxygen dihedral angle (the double bonded oxygen in this case), shown in Figure 5. The four most stable conformers all have dihedral angles of either 0 or 180; there is significant population found at other angles, for both classical MD and PIMD. The classical distribution is more sharply peaked than PIMD. Overall, the relative change in distributions between the PIMD and classical MD simulations appears to be smaller for glycine than for *s*-triazine, likely because glycine is not predominantly in its ground state at the sampled temperature.

The measured NEXAFS and ISEELS spectra of gaseous glycine evaporated at ~415˚C are shown in Figure 6, along with calculated spectra at the nitrogen K-edge using the different approaches to sample nuclear degrees of freedom; the experimental data are taken from the

literature.[17,36] The theoretical results are aligned with the experimental IP as described in Section 2. The NEXAFS spectrum of glycine consists of four features which have been assigned previously as follows: (1) a well resolved HOMO to LUMO feature assigned as σ^*_{NH}; (2) an easily distinguished feature assigned as π^*_{NC}; (3) a feature assigned as σ^*_{NC}; (4) a slightly more intense feature than feature 3 believed to be a Rydberg feature.[17,36] These assignments are likely an oversimplification, as it has been shown that motions in the molecule can cause these features to shift in energy and blend together.[3]

We will now discuss the accuracy of the theoretical approaches employed in this work for glycine. The lowest energy conformation (with fixed nuclei) produces the correct number of features with a similar intensity ratio as found in experiment; it is not possible to homogeneously broaden the spectrum to match experiment. This is almost certainly due to the lack of certain molecular conformations at the given experimental temperature. By Boltzmann weighting the four most populated conformers of glycine, one can obtain a spectrum that generates features 2, 3 and 4.[17] Feature 1 is split into two smaller features, once again likely due to a lack of sampling of less populated conformations. It appears that in order to accurately reproduce the spectrum of glycine, it is necessary to sample a wider variety of conformations. As shown previously, classical MD produces the correct number of features when a wider linewidth is used.[3] However, the relative intensities of features 3 and 4 are not well reproduced, nor is the correct spectral lineshape obtained. While this spectra is likely not fully converged, it appears close to convergence.

It was hoped that by using a quantum distribution of states generated by PIMD, a more accurate representation of the spectra would be obtained. While features 2, 3 and 4 are indeed more accurately reproduced than by any other method in terms of feature intensity and width, the

first feature is not resolved. The absence of the first feature cannot be attributed to the broadening scheme: if the broadening is narrowed further, too many features are obtained in this energy range and if broadening is increased, the whole region is flattened. We can only speculate that additional sampling would produce a more accurate spectrum, including feature 1. Unfortunately, it is not possible to converge the statistics of glycine when utilizing PIMD with only 100 configurations. Due to the wider variation of molecular configurations, it will take more configurations to converge a PIMD-sampled spectra than it does to converge a classical MD sampled spectra; this is evidenced by the larger spectral standard deviation associated with PIMD compared with that of classical MD. PIMD requires at least several hundred separate uncorrelated conformations to accurately sample the molecule, which, for now, is computationally inaccessible using our technique. We note that the classical MD spectra exhibits less variance than the PIMD spectra, which means it should take less sampling to converge.

Using classical MD to sample molecular configurations does not yield predictive results. It appears imperative to include quantum motion to accurately predict spectra, implying that a careful balance of adequate sampling and computational cost is required. One possible solution is that localized states, such as those producing features 1 and 2 could be accurately calculated using localized basis sets, significantly reducing the computational cost. We note that in going to more complicated systems, such as solvated systems, the ratio of the number of configurations needed to converge PIMD relative to the number of configurations needed to converge classical MD may decrease due to a lack of sharp features in the spectra of larger or more complicated systems.

If one were to use the estimates of bound state lifetime broadening of 0.1 eV for the lifetime broadening for bound states of nitrogen,[1] it quickly becomes apparent that motions are a large, and in certain cases, dominant, cause of peak widths. Within a certain simplification, the fixed-nuclei structure is the lifetime broadening limited spectra without motions. For glycine this is clearly not broad enough. In the case of *s*-triazine the first peak is too narrow, but we point out that there are Frank-Condon vibrational transitions which are also significant but our fixed-nuclei spectra will miss. It appears that most of the width of many of the bound peaks are caused by motion effects rather than lifetime effects. Lifetime widths only cause a fraction of the total width of any given bound peak, although that can change from a small fraction to a large fraction even within the same molecule (see features 1 and 4 of *s*-triazine). For unbound transitions, the distinction is less clear due to a less well known lifetime width, and likely larger lifetime broadening.

The conventional use of lifetime effects as an explanation of selective broadening appears to be an oversimplification. In certain cases, it is possible to broaden the spectra to obtain the correct general shape, but in other cases it simply is not possible, and nuclear motions must be invoked. In general, to accurately predict the spectral intensity and lineshape for light atoms it appears necessary to include both the effects of motion and lifetime. Our calculations on *s*-triazine which do not calculate lifetime broadening appear to do a reasonable job of predicting the spectra, leading us to speculate that motion effects are more important in general than an accurate knowledge of the lifetime broadening.

Molecular dynamics sampling is important for NEXAFS calculations because the time length of the x-ray probe is ultrashort, ca. tens of attoseconds. This is fast enough to "freeze out" the nuclear motions of the molecule. Subtle changes in molecular geometry evolve rapidly but

x-rays are fast enough to be sensitive to them. Other techniques with a longer measurement time scale (e.g vibrational spectroscopy) will average over molecular positions, meaning only part of the interaction time between the molecule and a photon will occur while the atoms are maximally displaced. Therefore, those techniques may not sample the strongest deviations from the mean positions.

4. Conclusions

The effect of including a quantum distribution of states in simulating the NEXAFS spectra of two isolated molecules was investigated. For *s*-triazine, a small highly symmetric aromatic molecule largely localized in its ground state, the changes observed by using a quantum distribution of states help explain the observed spectrum, in particular the asymmetry in observed features which could not be adequately explained by either classical MD sampling or fixed-nuclei data. The broadening of features appears, in large extent, to be driven by these vibrational motions, and in certain cases the vibrations are responsible for the observation of these features. This demonstrates the importance of both the Herzberg-Teller effect and of having a proper quantum distribution in order to accurately predict spectra of small molecules composed of light elements. This approach finds a much greater challenge with molecules that access a larger number of vibrational states; this is due to the difficulty in sampling an adequate number of conformations, as computational cost rises linearly with the number of configurations. Regardless, this accuracy is necessary for properly accounting for certain spectral features and indicates the hazards of drawing anything other than qualitative conclusions from calculations based on a single geometry, even for molecules in their ground vibrational state. As X-ray spectroscopy experiments continue to evolve and measurements become increasingly more

detailed, it is important to realize that these vibrational motions may comprise a natural limit to the resolution of NEXAFS and cannot be ignored. Thus, the ability to interpret these underlying vibrational motions will likely become increasingly important.

Acknowledgements

This work was supported by the Director, Office of Basic Energy Sciences, Office of Science, U.S. Department of Energy under Contract No. DE-AC02-05CH11231 through the LBNL Chemical Sciences Division, and the Molecular Foundry. Computational resources were provided by NERSC, a DOE Advanced Scientific Computing Research User Facility.

Figure and Table Captions

Table I. Calculated vibrational modes of *s*-triazine listed in frequency (cm^{-1}). The molecular structure was optimized and then the vibrational modes were calculated, using the B3LYP exchange-correlation functional and a 6-311G* basis set. We note that the lowest energy mode corresponds to ~ 450 K.

Table II. Calculated vibrational modes of glycine listed in both frequency (cm^{-1}) and temperature (K). The molecular structure was optimized and then the vibrational modes were calculated, using the B3LYP exchange-correlation functional and a 6-311G* basis set. The lowest energy mode corresponds to 92.97 K, well below experimental temperature.

Figure 1. Measured and simulated core-level spectra of s-triazine at the nitrogen K edge: (a) Measured NEXAFS (blue) and ISEELS (yellow) spectra in comparison with the calculated spectra using fixed nuclei (red), classical MD (black with grey error bars) and PIMD (purple with error bars). The average spectra for classical MD and PIMD are shown in darker colors with a shaded width of one standard deviation. The experimental spectra are taken from the literature and the vertical line is the experimental ionization potential (see text). (b) An enlargement of the spectral energy range 398-405 eV for PIMD, classical MD and NEXAFS data. The PIMD results reproduce a shoulder around 400eV, as found experimentally, unlike the classical MD results.

Table III. Summary of transition energies (eV) obtained by various methods for *s*-triazine.

Figure 2. Isosurfaces of several electronic states of s-triazine from the fixed nuclei structure without and with a core hole on the bottom most nitrogen and from a single PIMD configuration without and with a nitrogen 1s core excitation respectively. Positive and negative phases are indicated in red and green respectively. The excited nitrogen is always on the lowermost (blue) atom of the selected configuration. State A corresponds to spectral feature 1, state B spectral feature 2, state C is representative of spectral feature 3 and state D is a scattering state corresponding to feature 5. Further details are given in the text.

Figure 3. A plot of the difference in s-triazine CNC bond angles, with the two relevant angles labeled in red (θ_L and θ_R), sampled from the classical (blue) and PIMD (red) distributions. The PIMD data shows a significantly broader distribution than that of classical MD. The errors are of the size of the width of the lines.

Figure 4. A plot of s-triazine C-N-C-H dihedral angles, with relevant atoms labeled (1-4), sampled from classical (blue) and PIMD (red) distributions. The PIMD data shows a significantly broader distribution than that of classical MD. The errors are of the size of the width of the lines.

Figure 5. A plot of the glycine N-C-C=O dihedral angle, with the relevant atoms labeled (1-4), sampled from classical (blue) and PIMD (red) distributions. The PIMD data shows a slightly broader distribution than that of classical MD. The errors are of the size of the width of the lines.

Figure 6. Measured and simulated core-level spectra of glycine at the nitrogen K-edge: Measured NEXAFS (blue) and ISEELS (yellow) spectra in comparison with the calculated spectra using fixed nuclei (red), a Boltzmann-weighted average from the four lowest energy conformers (green), classical MD (black with grey error bars) and PIMD (purple with error bars). The average spectra for classical MD and PIMD are shown in darker colors with a shaded width of one standard deviation. The experimental spectra are taken from the literature and the vertical line is the experimental ionization potential (see text).

Figures and Tables

Vibrational modes of *s*-triazine

Index	Frequency (cm-1)
1	309.20
2	310.33
3	665.46
4	665.58
5	734.48
6	892.15
7	972.71
8	985.03
9	985.21
10	1115.53
11	1156.60
12	1157.04
13	1162.83
14	1349.93
15	1385.86
16	1386.23
17	1530.57
18	1531.12
19	3064.39
20	3064.69
21	3070.13

Table I

Vibrational modes of glycine

Index	Frequency (cm^{-1})
1	64.09
2	313.67
3	338.63
4	483.16
5	514.51
6	628.73
7	760.79
8	8357.35
9	889.82
10	1007.97
11	1042.23
12	1127.05
13	1144.61
14	1303.78
15	1304.06
16	1385.88
17	1449.56
18	1649.02
19	1726.91
20	2799.60
21	2994.08
22	3049.39
23	3438.68
24	3550.19

Table II

a)

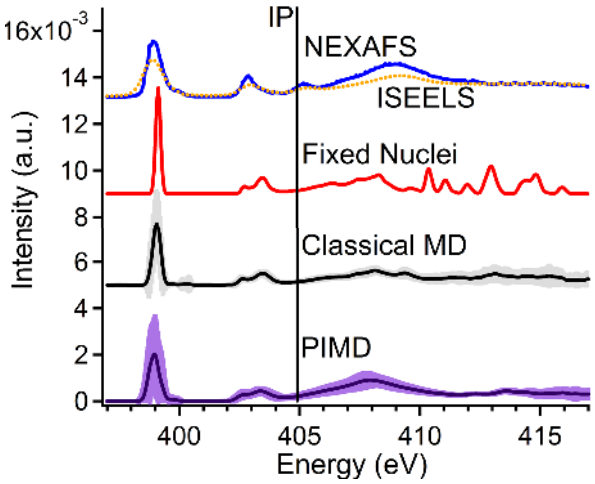
16x10-3
14
12
10
8
6
4
2
0
Intensity (a.u.)
IP
NEXAFS
ISEELS
Fixed Nuclei
Classical MD
PIMD
400
405
410
415
Energy (eV)

b)

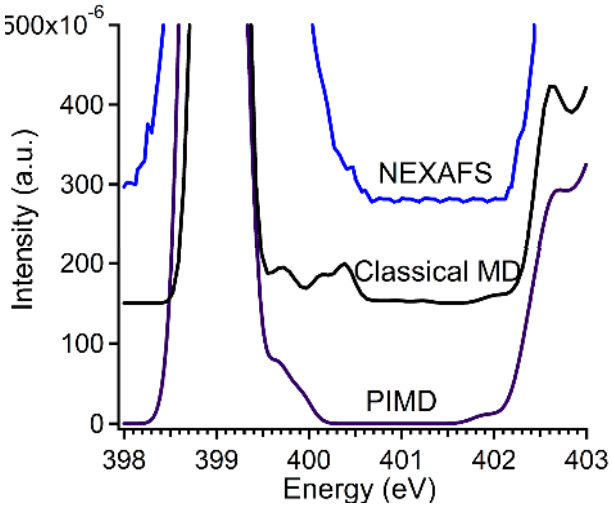
500x10-6
400
300
200
100
0
Intensity (a.u.)
NEXAFS
Classical MD
PIMD
398
399
400
401
402
403
Energy (eV)

Figure 1

s-triazine feature locations - energy (eV)

Feature number	NEXAFS	Fixed Nuclei	Classical MD	PIMD
1	398.9	399.2	399.1	398.9
2	399.9		~399.4	~399.8
3	402.9	~403.2	~403.1	~403.1
4	405.2			
5	409.0	~408.7	~408.2	~408.0
6	415.3		~413.5	~413.7

Table III

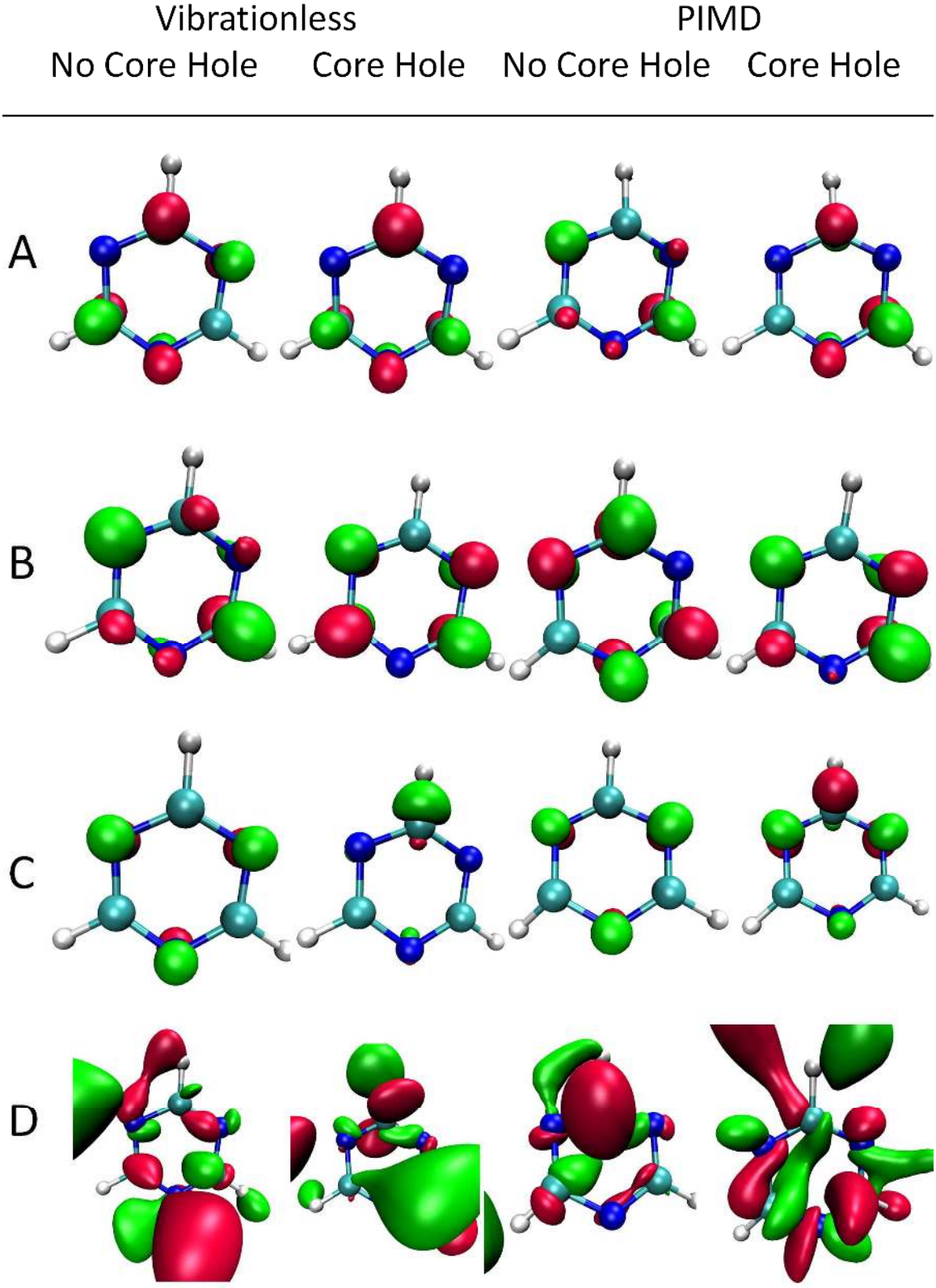
Vibrationless
PIMD
No Core Hole
Core Hole
No Core Hole
Core Hole
A
B
C
D

Figure 2

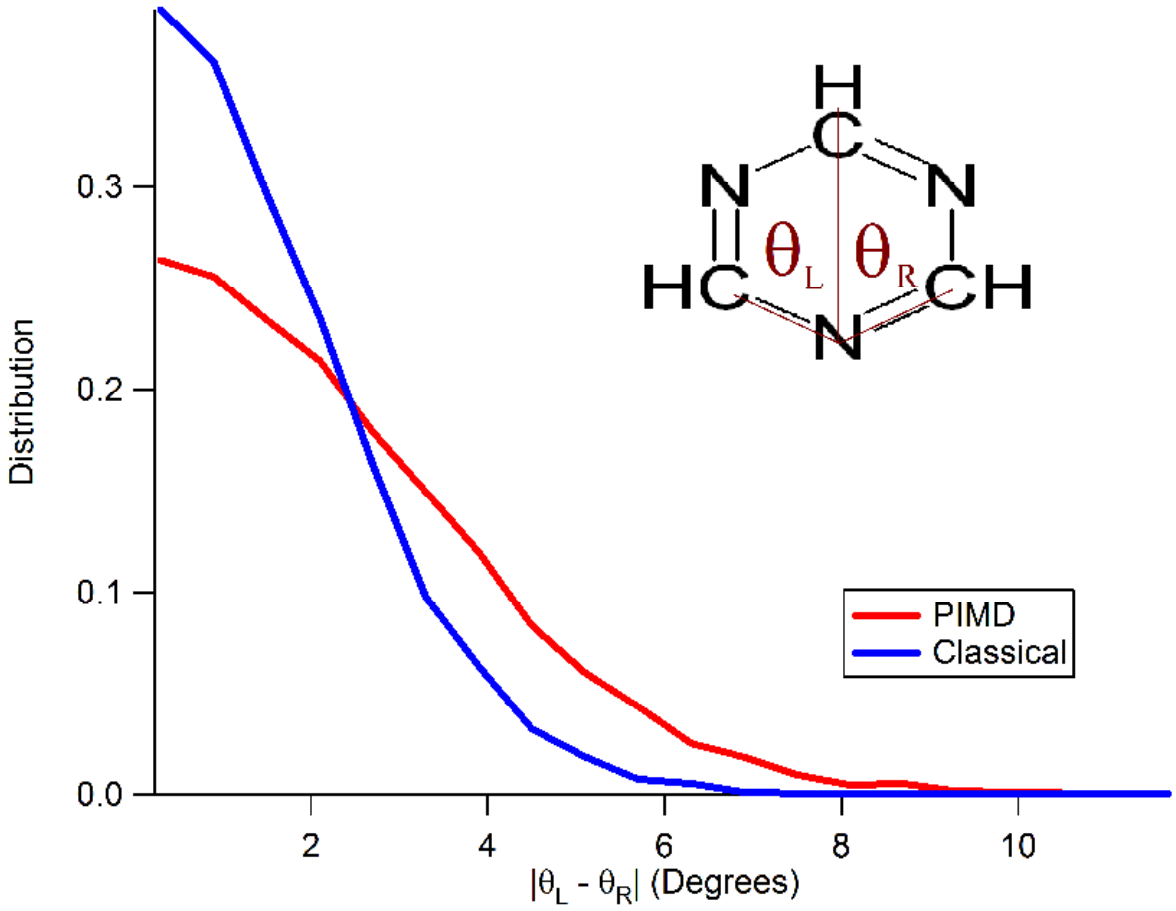

Figure 3

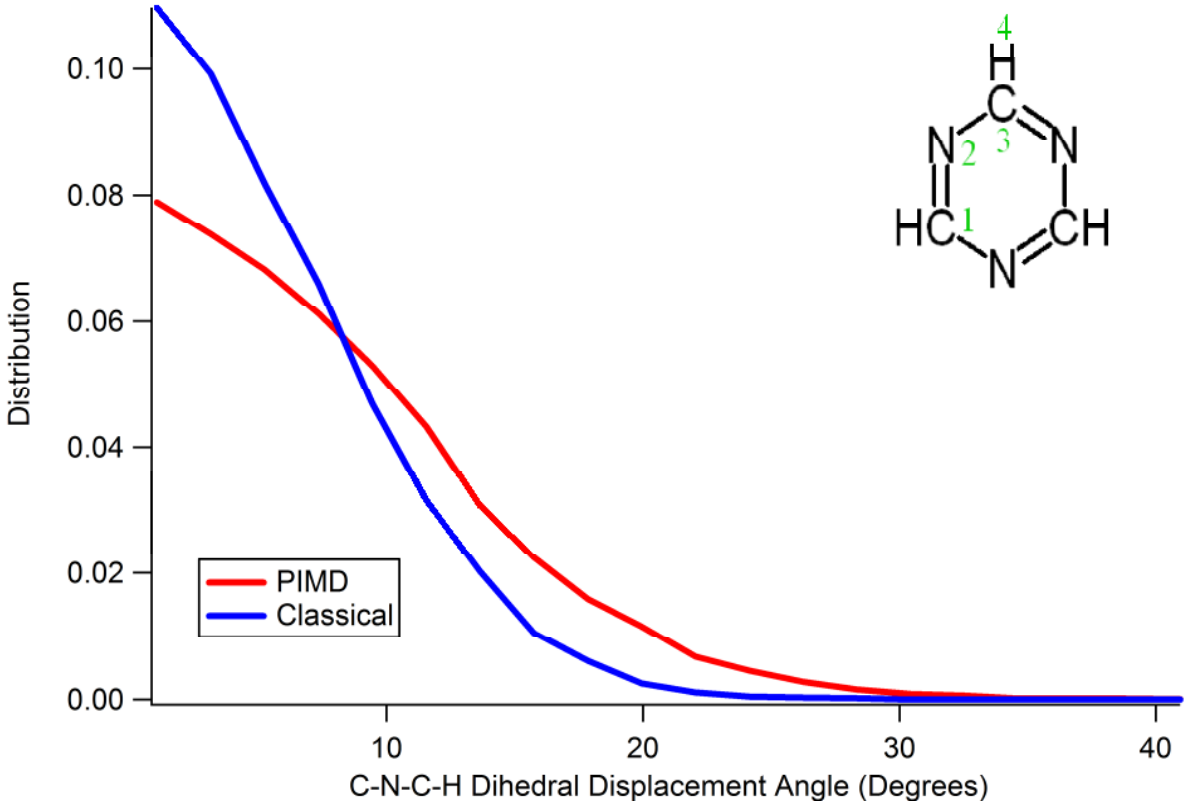
Distribution
0.10
0.08
0.06
0.04
0.02
0.00
10
20
30
40
C-N-C-H Dihedral Displacement Angle (Degrees)
PIMD
Classical
4
H
C
N
2
3
N
HC
1
CH
N

Figure 4

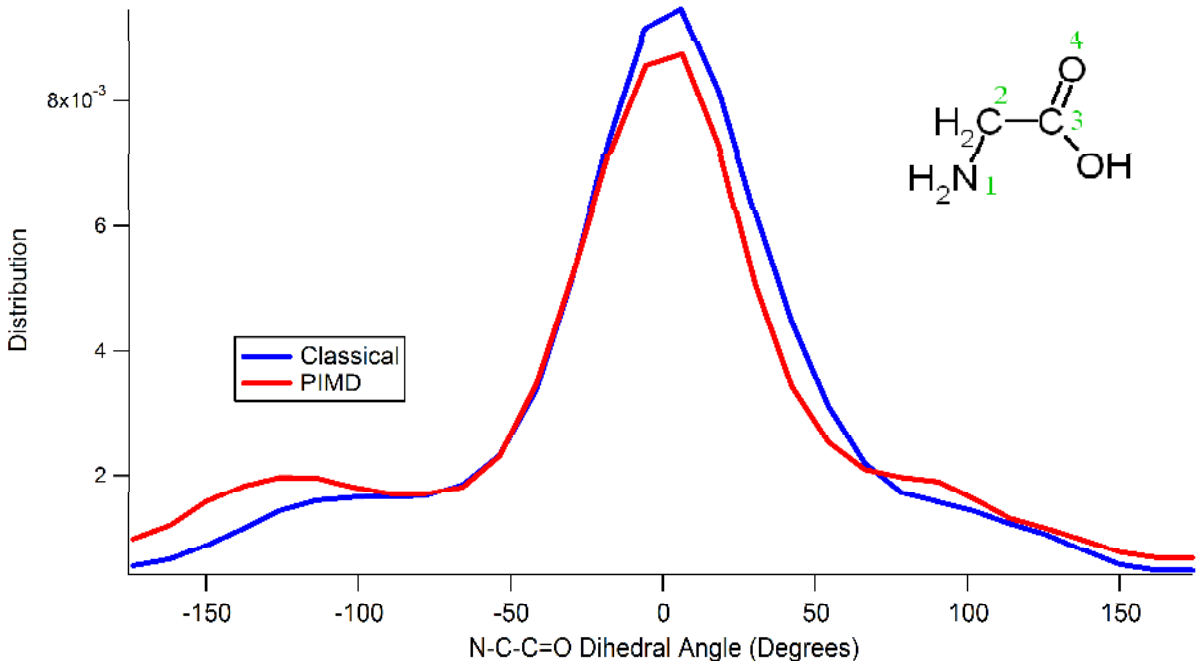
8x10-3
6
4
2
Distribution
Classical
PIMD
-150
-100
-50
0
50
100
150
N-C-C=O Dihedral Angle (Degrees)
H2C
H2N
OH
1
2
3
4

Figure 5

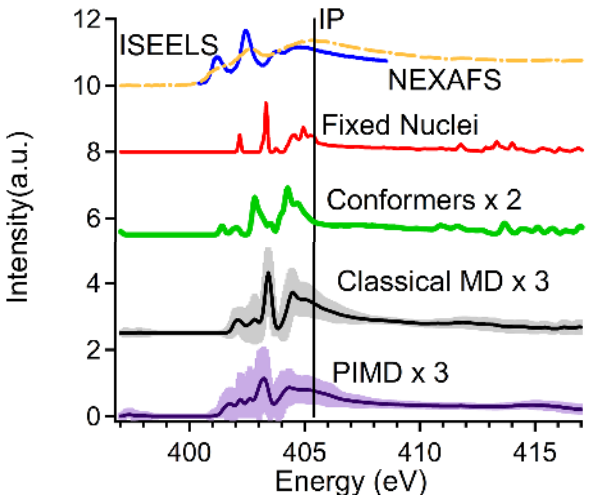
ISEELS
IP
NEXAFS
Fixed Nuclei
Conformers x 2
Classical MD x 3
PIMD x 3
Intensity(a.u.)
Energy (eV)
0
2
4
6
8
10
12
400
405
410
415

Figure 6

[1] J. Stöhr, *NEXAFS Spectroscopy*. (Springer, Berlin, 1992).
[2] J. Stewart-Ornstein, A. P. Hitchcock, D. H. Cruz, P. Henklein, J. Overhage, K. Hilpert, J. D. Hale, and R. E. W. Hancock, Journal of Physical Chemistry B **111** (26), 7691 (2007); H. Ade and A. P. Hitchcock, Polymer **49** (3), 643 (2008).
[3] J. S. Uejio, C. P. Schwartz, R. J. Saykally, and D. Prendergast, Chemical Physics Letters **467** (1-3), 195 (2008).
[4] P. Hohenberg and W. Kohn, Physical Review B **136** (3B), B864 (1964); W. Kohn and L. J. Sham, Physical Review **140** (4A), 1133 (1965).
[5] C. Kolczewski, R. Puttner, O. Plashkevych, H. Agren, V. Staemmler, M. Martins, G. Snell, A. S. Schlachter, M. Sant'Anna, G. Kaindl, and L. G. M. Pettersson, Journal of Chemical Physics **115** (14), 6426 (2001).
[6] D. Prendergast and G. Galli, Physical Review Letters **96** (21) (2006).
[7] Y. Luo, H. Agren, M. Keil, R. Friedlein, and W. R. Salaneck, Chemical Physics Letters **337** (1-3), 176 (2001).
[8] L. Triguero, L. G. M. Pettersson, and H. Agren, Physical Review B **58** (12), 8097 (1998).
[9] A. Nilsson and L. G. M. Pettersson, Surface Science Reports **55** (2-5), 49 (2004).
[10] J. J. Rehr and A. L. Ankudinov, Journal of Synchrotron Radiation **10**, 43 (2003).
[11] E. L. Shirley, Physical Review Letters **80** (4), 794 (1998).
[12] D. Duflot, K. Sidhoum, J. P. Flament, A. Giuliani, J. Heinesch, and M. J. Hubin-Franskin, European Physical Journal D **35** (2), 239 (2005).
[13] H. Agren, V. Carravetta, O. Vahtras, and L. G. M. Pettersson, Chemical Physics Letters **222** (1-2), 75 (1994).
[14] U. Ekstrom, P. Norman, V. Carravetta, and H. Agren, Physical Review Letters **97** (14) (2006).
[15] A. L. Ankudinov and J. J. Rehr, Journal of Synchrotron Radiation **10**, 366 (2003).
[16] G. Vall-llosera, B. Gao, A. Kivimaeki, M. Coreno, J. A. Ruiz, M. de Simone, H. Agren, and E. Rachlew, Journal of Chemical Physics **128** (4) (2008).
[17] M. L. Gordon, G. Cooper, C. Morin, T. Araki, C. C. Turci, K. Kaznatcheev, and A. P. Hitchcock, Journal of Physical Chemistry A **107** (32), 6144 (2003).
[18] I. Minkov, F. Gel'mukhanov, H. Agren, R. Friedlein, C. Suess, and W. R. Salaneck, Journal of Physical Chemistry A **109** (7), 1330 (2005).
[19] G. Herzberg and E. Teller, Zeitschrift Fur Physikalische Chemie-Abteilung B-Chemie Der Elementarprozesse Aufbau Der Materie **21** (5/6), 410 (1933).
[20] F. D. Vila, J. J. Rehr, H. H. Rossner, and H. J. Krappe, Physical Review B **76** (1) (2007); H. H. Rossner, D. Schmitz, P. Imperia, H. J. Krappe, and J. J. Rehr, Physical Review B **74** (13) (2006).
[21] C. Chakravarty, International Reviews in Physical Chemistry **16** (4), 421 (1997).
[22] F. Della Sala, R. Rousseau, A. Gorling, and D. Marx, Physical Review Letters **92** (18) (2004).
[23] A. Kaczmarek, M. Shiga, and D. Marx, The Journal of Physical Chemistry A **113** (10), 1985 (2009).
[24] J. P. Perdew, K. Burke, and M. Ernzerhof, Physical Review Letters **77** (18), 3865 (1996).
[25] P. E. Blochl, Physical Review B **50** (24), 17953 (1994).

[26] B. Hetenyi, F. De Angelis, P. Giannozzi, and R. Car, Journal of Chemical Physics **120** (18), 8632 (2004).
[27] S. Baroni, A. D. Corso, S. D. Gironcoli, and P. Giannozzi, PWSCF (2008).
[28] D. Prendergast, J. C. Grossman, and G. Galli, Journal of Chemical Physics **123** (1) (2005).
[29] E. L. Shirley, Physical Review B **54** (23), 16464 (1996).
[30] T. A. D. D.A. Case, T.E. Cheatham, III, C.L. Simmerling, J. Wang, R.E. Duke, R., K. M. M. Luo, D.A. Pearlman, M. Crowley, R.C. Walker, W. Zhang, B. Wang, S., A. R. Hayik, G. Seabra, K.F. Wong, F. Paesani, X. Wu, S. Brozell, V. Tsui, H., L. Y. Gohlke, C. Tan, J. Mongan, V. Hornak, G. Cui, P. Beroza, D.H. Mathews, C., and W. S. R. Schafmeister, and P.A. Kollman, (2006); J. M. Wang, W. Wang, P. A. Kollman, and D. A. Case, Journal of Molecular Graphics & Modelling **25** (2), 247 (2006).
[31] M. J. T. Frisch, G. W.; Schlegel, H. B.; Scuseria, G. E.; Robb, M. A.; Cheeseman, J. R.; Montgomery, Jr., J. A.; Vreven, T.; Kudin, K. N.; Burant, J. C.; Millam, J. M.; Iyengar, S. S.; Tomasi, J.; Barone, V.; Mennucci, B.; Cossi, M.; Scalmani, G.; Rega, N.; Petersson, G. A.; Nakatsuji, H.; Hada, M.; Ehara, M.; Toyota, K.; Fukuda, R.; Hasegawa, J.; Ishida, M.; Nakajima, T.; Honda, Y.; Kitao, O.; Nakai, H.; Klene, M.; Li, X.; Knox, J. E.; Hratchian, H. P.; Cross, J. B.; Bakken, V.; Adamo, C.; Jaramillo, J.; Gomperts, R.; Stratmann, R. E.; Yazyev, O.; Austin, A. J.; Cammi, R.; Pomelli, C.; Ochterski, J. W.; Ayala, P. Y.; Morokuma, K.; Voth, G. A.; Salvador, P.; Dannenberg, J. J.; Zakrzewski, V. G.; Dapprich, S.; Daniels, A. D.; Strain, M. C.; Farkas, O.; Malick, D. K.; Rabuck, A. D.; Raghavachari, K.; Foresman, J. B.; Ortiz, J. V.; Cui, Q.; Baboul, A. G.; Clifford, S.; Cioslowski, J.; Stefanov, B. B.; Liu, G.; Liashenko, A.; Piskorz, P.; Komaromi, I.; Martin, R. L.; Fox, D. J.; Keith, T.; Al-Laham, M. A.; Peng, C. Y.; Nanayakkara, A.; Challacombe, M.; Gill, P. M. W.; Johnson, B.; Chen, W.; Wong, M. W.; Gonzalez, C.;Pople, J. A.;, Gaussian 03 (Gaussian, Inc., Wallingford, CT, 2004).
[32] R. Ramirez, C. P. Herrero, and E. R. Hernandez, Physical Review B **73** (24) (2006); D. Marx, M. E. Tuckerman, J. Hutter, and M. Parrinello, Nature **397** (6720), 601 (1999).
[33] S. Raugei and M. L. Klein, Chemphyschem **5** (10), 1569 (2004); U. W. Schmitt and G. A. Voth, Journal of Chemical Physics **111** (20), 9361 (1999).
[34] T. F. Miller and D. C. Clary, Physical Chemistry Chemical Physics **6** (10), 2563 (2004).
[35] E. Apen, A. P. Hitchcock, and J. L. Gland, Journal of Physical Chemistry **97** (26), 6859 (1993).
[36] O. Plekan, V. Feyer, R. Richter, M. Coreno, M. de Simone, K. C. Prince, and V. Carravetta, Journal of Electron Spectroscopy and Related Phenomena **155** (1-3), 47 (2007).